Thin Solid Films 595 (2015) 226–230

Contents lists available at ScienceDirect

Thin Solid Films

journal homepage: www.elsevier.com/locate/tsf

Optimization of hydrogenated amorphous silicon germanium thin films and solar cells deposited by hot wire chemical vapor deposition

L.W. Veldhuizen [a,*], C.H.M. van der Werf [b], Y. Kuang [a], N.J. Bakker [b], S.J. Yun [c], R.E.I. Schropp [a,b]

[a] Eindhoven University of Technology (TU/e), Department of Applied Physics, Plasma & Materials Processing, P.O. Box 513, 5600 MB Eindhoven, The Netherlands
[b] Energy Research Center of the Netherlands (ECN), ECN-Solliance, High Tech Campus Building 21, 5656 AE Eindhoven, The Netherlands
[c] Thin Film Solar Cell Technology Team, Convergence Components and Materials Research Laboratory, Electronics and Telecommunications Research Institute (ETRI), 218 Gajeongno, Yuseong-gu, Daejeon 305-700, Republic of Korea

ARTICLE INFO

Article history:
Received 6 February 2015
Received in revised form 4 May 2015
Accepted 25 May 2015
Available online 28 May 2015

Keywords:
Amorphous silicon germanium
Hot wire chemical vapor deposition
Solar cells
Ambipolar diffusion length

ABSTRACT

This work studies hydrogenated amorphous silicon germanium films, deposited by hot wire chemical vapor deposition, to be used as low band gap absorber material in thin film solar cells. Material properties, such as the bonding configurations, the ambipolar diffusion length and the optical band gap, were examined as a function of the substrate temperature and germanium content. Our best materials were incorporated in single junction solar cells with high long-wavelength response and a tandem solar cell with an efficiency of 10.42%.

1. Introduction

Hydrogenated amorphous silicon germanium (a-SiGe:H) is a low band gap semiconductor that can be used as active material in thin film silicon based solar cells. The direct nature of its band gap allows for the use of a very thin absorber layer and much shorter deposition times compared to microcrystalline silicon (μc Si:H). In the past, United Solar Ovonic has developed a-SiGe:H in triple junction solar cells [1]. However, the high defect density of low band gap a-SiGe:H films deposited by plasma enhanced chemical vapor deposition (PECVD), the occurrence of light induced degradation of devices with relatively thick absorber layers in particular and the high costs of Ge-containing source gasses, have thus far prevented a-SiGe:H in thin film silicon based solar cells to be viable. On the other hand, the amorphous nature of a-SiGe:H makes it easier to achieve conformal growth of thin films on rough or nanostructured surfaces than is the case with μc-Si:H. Combined with the relatively high deposition rate of hot wire chemical vapor deposition (HWCVD) as compared to PECVD, HWCVD a-SiGe:H is a feasible option for thin film silicon PV on textured light-scattering substrates. The recent developments in advanced light-scattering structures such as textures created with nano-imprint lithography [2] and naturally grown ZnO nanorods [3], have motivated us to investigate whether a-SiGe:H HWCVD can be considered as active material for low cost thin film multijunction solar cells. Earlier work by NREL has shown that HWCVD produces a-SiGe:H material with superior quality compared to that deposited by PECVD, in particular for films with high germanium content. That work resulted in an 8.64% single junction cell without any band-gap profiling in the absorber layer [4]. In this paper we show that we have further advanced the performance of cells. In particular, an a-Si:H/a-SiGe:H tandem cell with HWCVD a-SiGe:H layer has been fabricated.

2. Experiment

All a-SiGe:H films in this study were fabricated by HWCVD using two parallel 0.3-mm diameter Ta filaments that were resistively heated to a temperature of 1700°C during deposition. Besides being heated by the filaments, substrates were heated at the back side using ex vacuo heating elements. Compared to our previous study [5], the filament to substrate distance was reduced from 55 mm to 35 mm, allowing for higher reaction pressures and higher gas flows, and thus, lower gas depletion. We also altered our Ge source gas mixture to 30% GeH_4 diluted in H_2 instead of 10% in He, enabling a lower GeH_4 depletion and ruling out the influence of helium during the growth process. High purity SiH_4 was used as Si source gas. The processing pressure was kept at 2 Pa, and the pre-deposition background pressure was $<10^{-5}$ Pa. Generally for these films, a high deposition rate of 0.5 nm/s is obtained. For material analysis, films of 200 nm were deposited on both Corning EAGLE XG glass and natively oxidized polished c-Si wafers. The films deposited on c-Si wafers were used for Fourier transform infrared (FTIR)

* Corresponding author at: De Rondom 70, 5612 AP, P.O. Box 513, FLUX 3.096, 5600 MB Eindhoven, The Netherlands.
E-mail address: l.w.veldhuizen@tue.nl (L.W. Veldhuizen).

http://dx.doi.org/10.1016/j.tsf.2015.05.055

spectroscopy analysis with which the hydrogen concentration C_H, microstructure parameter R^* (the contribution of Si-H_2 bonds versus Si-H bonds) and preferential attachment ratio of hydrogen to silicon P_{Si} (Si-H bonds versus Ge–H bonds, weighted with the Ge content) were determined using methods as described in our previous work [5]. Raman spectroscopy using a 514.5 nm Ar^+ laser was employed to derive the Ge content C_{Ge} in the films; this method was calibrated with X-ray photoelectron spectroscopy [5,6]. The thickness and optical constants of the films were determined with reflection and transmission measurements in combination with the O'Leary–Johnson–Lim model [7]. As a value for the optical band gap we use the photon energy $E_{3.5}$, defined as the energy at which the absorption coefficient α is $10^{3.5}$ cm^{-1}. For our films, the value of $E_{3.5}$ is similar to that of the Tauc band gap but its experimental determination is less ambiguous [8]. In the characterization of the layers we put emphasis on the photoelectrical performance. For these measurements, two coplanar Ag electrodes were deposited by thermal evaporation. The photoconductivity (measured under AM1.5 illumination and in air ambient) and the dark conductivity (measured in vacuum), were used to determine the photosensitivity. The steady-state-photograting technique with a 10 mW/cm^2 HeNe laser was applied to obtain the ambipolar diffusion length L_d, dominated by the length of the diffusion path of the photogenerated minority carriers [9,10]. The current density–voltage (J–V) characteristics of solar cells is measured under a Wacom dual source solar simulator, calibrated to the AM1.5 spectrum.

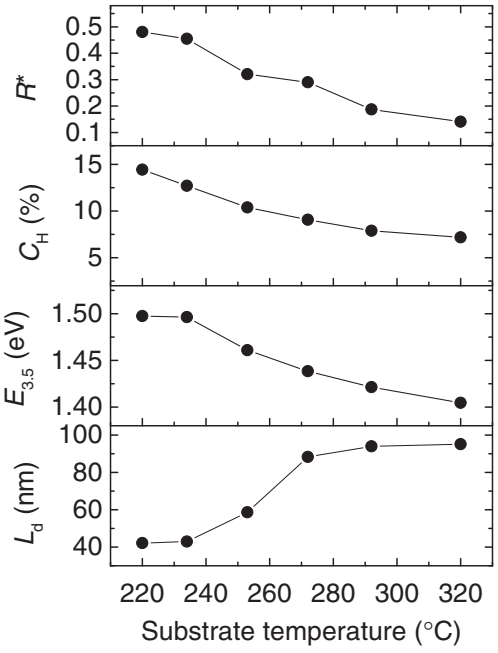

Fig. 1. Material parameters of a-SiGe:H layers as a function of the substrate temperature during the deposition. From top to bottom: microstructure parameter (R^*), hydrogen concentration (C_H), optical band gap ($E_{3.5}$) and ambipolar diffusion length (L_d).

3. Results and discussion

3.1. The influence of the substrate temperature

In order to investigate the effect of the substrate temperature, six a-SiGe:H films were deposited using various levels of additional ex vacuo heating at the rear of the sample, resulting in substrate temperatures varying between 220°C and 320°C. Preceding every deposition, the Corning glass and c-Si wafer substrates were preheated for 1 h in the reactor while being shielded from the heated filaments by a shutter plate. The precursor flows were set at 50.4 sccm of SiH_4 and 78.9 sccm of the GeH_4 diluted in H_2. This resulted in films with an atomic Ge content of 55% ± 2%, showing no dependence on the substrate temperature. Fig. 1 presents the material parameters that do show a clear trend with the substrate temperature. The microstructure parameter R^*, as measured with FTIR, shows a considerable decrease from 0.45 to 0.14 with increasing substrate temperature. The decrease of R^* indicates that, as the substrate temperature is increased, less hydrogen is present in the form of SiH_2 or on the inner surface of voids in the material. This trend has also been observed in a-Si:H films and can be explained by the higher mobility of growth radicals at surfaces at an elevated substrate temperature, resulting in the growth of a more compact material [11]. Although R^* is mainly associated with the quality of a-Si:H films and devices, the reduction of R^* was also found to have a positive effect on the a-SiGe:H device performance in earlier work by NREL [4]. The decrease of C_H from 14.4% to 7.2% shows that, as the substrate temperature increases, less hydrogen is incorporated in the material. We believe that this decrease is also the main reason for the optical band gap $E_{3.5}$ to drop by 0.1 eV. Since a thin film silicon based device partly relies on diffusion in order for the charge carriers to be collected, it is desirable that the ambipolar diffusion length L_d in the intrinsic layer is close to the thickness of the intrinsic layer. As is shown in Fig. 1, the increased deposition temperature causes the L_d to be more than doubled, from a value of 42 nm, close to the detection limit, to a value of 95 nm. This boost in electrical quality seems to be related to the reduction of R^*, as has also been observed for unalloyed a-Si:H films [11]. The material quality is thus significantly increased when using an elevated substrate temperature. And although these results would entice us to use the highest possible substrate temperature for the deposition of a-SiGe:H in our devices, also the thermal stability of the underlying (doped) layers and metal layers in the devices has to be taken into account. For this reason, we choose to deposit the remaining a-SiGe:H layers in this study at a substrate temperature of 272°C.

3.2. Controlling germanium content of a-SiGe:H

In the previous section, we have only considered a-SiGe:H films with a Ge content of approximately 55%. Next, we proceed by varying the GeH_4 gas flow ratio $X_{GeH4} = [GeH_4/(GeH_4 + SiH_4)]$ in order to deposit films with various Ge contents. Earlier work on a-SiGe:H films deposited by HWCVD suggested that high depletion of the GeH_4 results in degraded material quality [4]. We therefore maximized the GeH_4 flow at every flow ratio X_{GeH4}. Fig. 2 gives an overview of Raman spectra of the Ge–Ge, Si–Ge and Si–Si TO phonons of a-SiGe:H in an entirely amorphous phase (270 cm^{-1}, 375 cm^{-1} and 480 cm^{-1} respectively) and FTIR spectra of the Ge–H, Si–H and Si–H_2 stretching modes (1880 cm^{-1}, 2000 cm^{-1} and 2090 cm^{-1} respectively). In between these two figure panels, the values of both the GeH_4 flow ratio X_{GeH4} and the corresponding Ge content C_{Ge} are shown, the latter of which is calculated using the Ge–Ge, Si–Ge Raman TO peak intensities [6]. The values for C_{Ge} and X_{GeH4} are not exactly linearly correlated, which indicates that Ge is preferentially incorporated in the a-SiGe:H films. This behavior can be explained by preferential dissociation of GeH_4 over SiH_4 due to the weaker bonding strength of Ge–H compared to Si–H, and by the lower mobility of Ge–H_x radicals on the surface [12,13]. As C_{Ge} increases, the Raman and FTIR spectra show a smooth transition from contributions of Si bonds to those of Ge bonds. With increasing Ge content, the Si–Si TO peak position shifts to lower wavenumbers due to the nearby presence of the heavier Ge atoms. The Ge–Ge TO peak position follows an opposite trend.

The FTIR spectra, as shown in Fig. 2, already provide qualitative insight into the development of the microstructure factor R^* and the preferential attachment factor P_{Si} [14]. Fig. 3 gives a quantitative overview of R^*, P_{Si} and other parameters as a function of the Ge content. R^* reaches its maximum value of 0.30 when the Ge content in the films is approximately 50%. When even more Ge is incorporated in the film, the homogeneity of the material increases again and R^* is reduced, reaching values that are lower than those reported for a-SiGe:H with similar

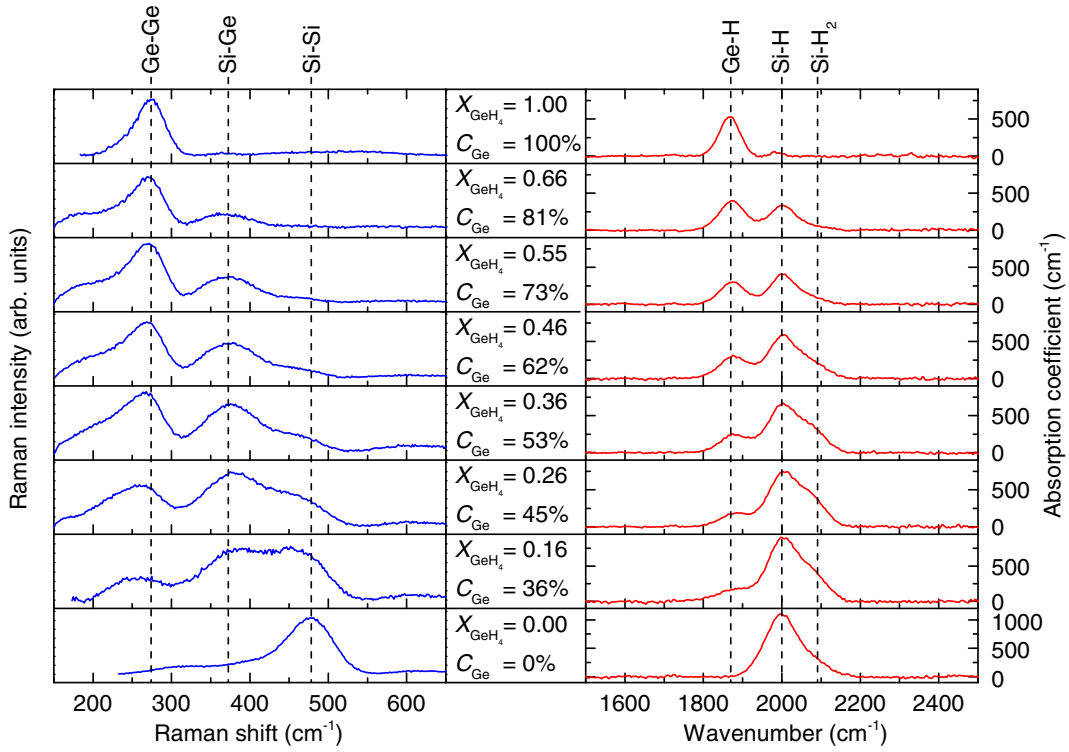

Fig. 2. Left: Raman spectra of the Si–Si, Si–Ge and Ge–Ge TO phonon peaks. Right: FTIR spectra of Ge and Si hydride stretching modes. The center column shows the corresponding GeH_4 gas flow ratio X_{GeH4} during deposition and the atomic Ge content C_{Ge} in the films.

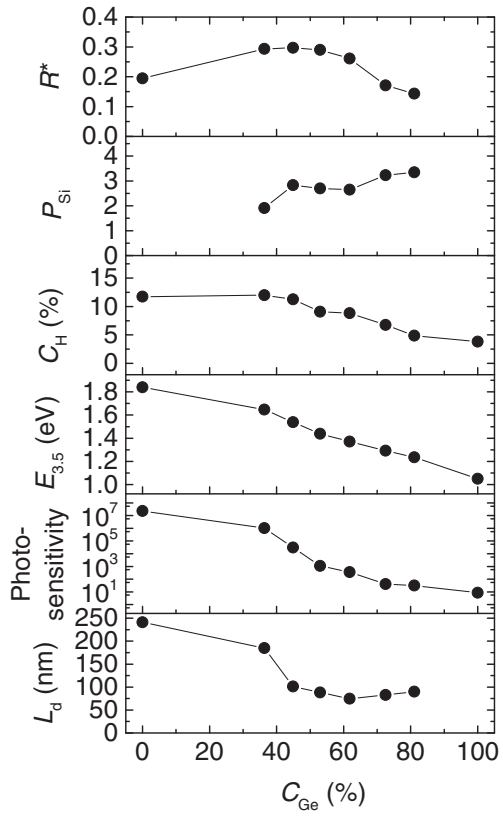

Fig. 3. Various material parameters as function of the Ge content. From top to bottom: microstructure parameter (R^*), preferential attachment of H to Si (P_{Si}), hydrogen concentration (C_H), optical band gap ($E_{3.5}$), photosensitivity and ambipolar diffusion length (L_d).

C_{Ge} deposited by PECVD [15,16]. The preferential attachment of H to Si, that originates from the lower bonding energy of Ge–H compared to Si–H, increases with C_{Ge}. This is undesirable, since high values of P_{Si} have been associated with high concentrations of Ge dangling bonds [14]. On the other hand, the values of P_{Si} are comparable to other values reported for a-SiGe:H deposited by HWCVD and are about a factor of 2 lower than values reported for a-SiGe:H deposited by PECVD [13]. The weaker Ge–H bond can also explain the decline of C_H for higher C_{Ge}, resulting in C_H = 4.9% for the a-Ge:H film (C_{Ge} = 100%). The optical band gap $E_{3.5}$ decreases almost linearly with C_{Ge}, varying from 1.84 eV for a-Si:H to 1.05 eV for a-Ge:H. The photosensitivity drops drastically with increasing C_{Ge}, mainly due to an increase in dark conductivity, which in turn can be explained by the decrease of the band gap. These values are in agreement with previously reported photosensitivities for both PECVD and HWCVD a-SiGe:H [13]. As expected, the ambipolar diffusion length L_d also diminishes as the films contain more Ge. However, the value stabilizes at around 80 nm for C_{Ge} > 60%, which is particularly useful for narrow-bandgap solar cells. At the ultimate end of the composition range (C_{Ge} = 100%), the photosensitivity of the a-Ge:H film was insufficient to measure the diffusion length properly. We believe that the reduced microstructure of films with high Ge content more than compensates the effect of the higher Ge dangling bond density. Still, L_d of our films with the highest Ge content is approximately 3 times lower than that of our a-Si:H film. As we will demonstrate in the following section, this does not have to be an obstacle for the fabrication of low band gap a-SiGe:H solar cells, since the high absorption coefficients of low band gap a-SiGe:H allow for a greatly reduced thickness of the intrinsic layer.

3.3. a-SiGe:H single junction solar cells

We now turn to incorporating two different a-SiGe:H intrinsic layers into single junction *n-i-p* devices. Three types of devices were made

using Asahi-U glass substrates, overcoated with Ag/ZnO:Al to replicate the typical morphology of Asahi U-type texture. A 27-nm thick a-Si:H *n*-type layer and a 26-nm thick nc-Si:H *p*-type layer were used, made by RF PECVD. As intrinsic layer, a 120-nm HWCVD a-SiGe:H layer with a 1.65 eV band gap or a 90-nm HWCVD a-SiGe:H layer with a 1.37 eV band gap was used. A 200-nm RF PECVD a-Si:H *i*-layer was used for a reference cell. The a-SiGe:H layers were embedded between thin a-Si:H PECVD buffer layers in order to reduce the defect density near the doped layers. The *p*-layer was deposited on a porous 1.8-nm buffer layer to provoke early onset of crystallinity. Pads of 80 nm thick sputtered tin-doped indium oxide (ITO) and 500-nm thick evaporated Ag contact grids define the cell active area of 0.13 cm^2. We have explored the external quantum efficiency (EQE) under short-circuit conditions of the three different solar cells. Fig. 4 shows the increasing long-wavelength response in the EQE as Ge is added to the intrinsic layer and its band gap becomes narrower. Even with the relatively thick *p*-layers, causing parasitic absorption at short wavelengths, the EQE of the 1.65 eV and 1.37 eV band gap a-SiGe:H cells translates into high current densities of respectively 17.9 mA/cm^2 and 23.1 mA/cm^2, compared to a current density of 14.3 mA/cm^2 for the a-Si:H reference cell. Furthermore, the device with the 90-nm thick a-SiGe:H layer and 1.37 eV band gap shows an EQE of 40% at a wavelength of 900 nm. This response at 900 nm exceeds that of the current world record efficiency μc-Si:H cell, which has an *i*-layer with a thickness of 1.8 μm. It should be noted that this PECVD layer requires a deposition time of over 3 h [17]. In contrast, the 90 nm thick *i*-layer of the HWCVD a-SiGe:H cell is deposited in 3 min only. For these a-SiGe:H single junction cells, no band gap profiling was applied and only limited effort was done to carry out the required optimization of the buffer layers and *p*-type layer. This is why the *J*-*V* characteristics for the 1.37 eV band gap cell shown in Fig. 4 were unoptimized (S-shape behavior).

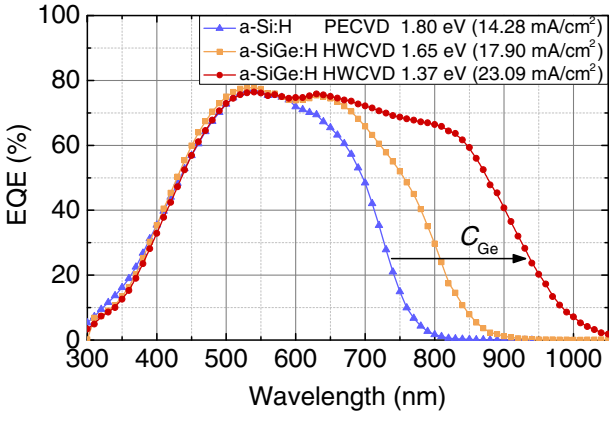

Fig. 4. External quantum efficiency (EQE) of two a-SiGe:H single junction solar cells, showing enhanced long-wavelength response compared to an a-Si:H cell made by PECVD.

3.4. a-Si:H/a-SiGe:H tandem solar cell

We fabricated a PECVD a-Si:H/HWCVD a-SiGe:H tandem cell. Again, the substrate used was an Asahi U-type glass with an Ag/ZnO:Al back contact. The bottom cell is similar to the single junction 1.37 eV band gap cell but this time band gap profiling was used at the back and front interface to avoid S-shape behavior of the *J*–*V* characteristics. The layer with the lowest band gap is 30 nm thick and positioned 15 nm from the *i*/*p* interface. The tunnel-recombination junction was finished by depositing a 20-nm nc-Si:H *n*-layer. The top cell absorber was a 200-nm PECVD *i*-layer. The top cell was completed by deposition of a 21-nm nc-Si:H *p*-layer, again on a 1.8-nm porous buffer layer. Finally, 80 nm ITO and an Ag grid were used. The *J*–*V* curve and the EQE of this tandem cell are shown in Fig. 5. From the EQE it is immediately clear that the top cell is current limiting. Nevertheless, the initial efficiency of the device is 10.42% (open-circuit voltage (V_{oc}) = 1.24 V, short-circuit current density (J_{sc}) = 12.3 mA/cm^2, fill factor (*FF*) = 0.682). The short-circuit density J_{sc}, as measured under the solar simulator, is higher than that derived from the EQE of the current limiting top cell. This discrepancy may be caused by current collection from outside the perimeter of the ITO window contact during the *J*–*V* measurement and a possible bias light dependency of the EQE [18]. We believe that the tandem cell performance can be significantly enhanced by improved photocurrent matching between the top and bottom cell, by incorporating SiO_x doped layers, by using a more transparent front TCO, and by optimizing the light scattering substrate.

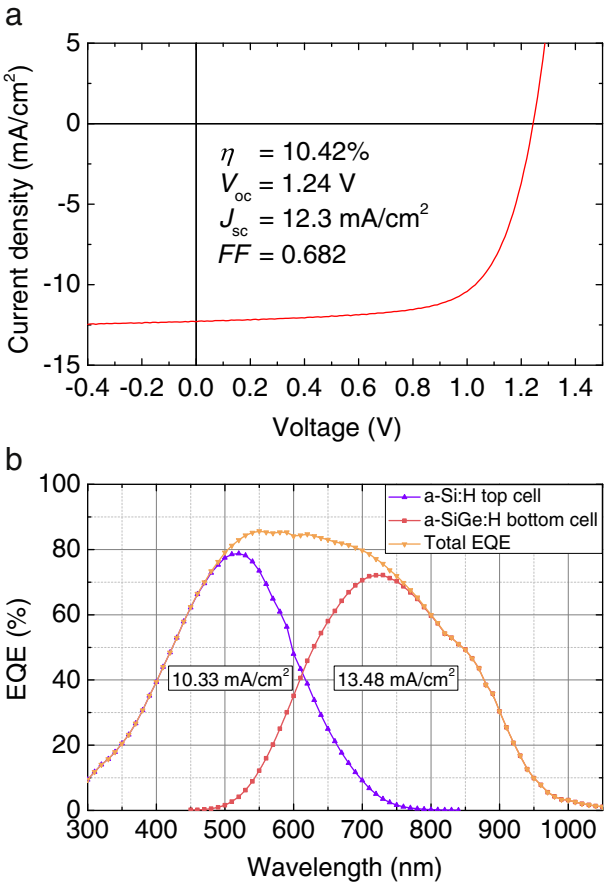

Fig. 5. *J*–*V* curve characteristic (a) and external quantum efficiency (EQE) (b) of a PECVD a-Si:H/HWCVD a-SiGe:H tandem cell.

4. Conclusions

In this work, the material properties of a-SiGe:H films deposited by HWCVD have been studied. It is shown that the material quality of a-SiGe:H films with a Ge content of 55% was improved when the substrate temperature was increased from 220°C to 320°C. We found that the ambipolar diffusion length L_d stabilizes at 80 nm for Ge contents larger than 60%. The optimized a-SiGe:H films were incorporated in *n*–*i*–*p* solar cells and an EQE value of 40% at a wavelength of 900 nm was realized. The *i*-layer of the cell has a band gap of 1.37 eV, a thickness of 90 nm and was deposited in just 3 min, which creates significant economic advantage with respect to cells deposited by PECVD. As a first attempt, an initial efficiency of 10.42% was demonstrated for a PECVD a-Si:H/HWCVD a-SiGe:H tandem cell.

Acknowledgments

The authors would like to acknowledge the support of the Energy International Collaboration Project (contract no. 2011-8520010-040) of the Korea Institute of Energy Technology Evaluation and Planning (KETEP) and NanoNextNL (project 02A.03), a micro and nanotechnology consortium of the government of the Netherlands and 130 partners. Also, we would like to thank Dr. J.K. Rath for managing the HWCVD facility used in this study.

References

[1] S. Guha, D. Cohen, E. Schiff, P. Stradins, P.C. Taylor, J. Yang, Industry–academia partnership helps drive commercialization of new thin-film silicon technology, Photovoltaics. Int. 13 (2011) 134–140.
[2] C. Battaglia, C.M. Hsu, K. Söderström, J. Escarré, F.-J. Haug, M. Charrière, M. Boccard, M. Despeisse, D.T.L. Alexander, M. Cantoni, Y. Cui, C. Ballif, Light trapping in solar cells: can periodic beat random? ACS Nano 6 (3) (2012) 2790–2797.
[3] Y. Kuang, C.H.M. van der Werf, Z.S. Houweling, R.E.I. Schropp, Nanorod solar cell with an ultrathin a-Si:H absorber layer, Appl. Phys. Lett. 98 (2011) 113111.
[4] A.H. Mahan, Y. Xu, L.M. Gedvilas, D.L. Williamson, A direct correlation between film structure and solar cell efficiency for HWCVD amorphous silicon germanium alloys, Thin Solid Films 517 (2009) 3532–3535.
[5] L.W. Veldhuizen, Y. Kuang, N.J. Bakker, C.H.M. van der Werf, S.-J. Yun, R.E.I. Schropp, Hydrogenated amorphous silicon germanium by Hot Wire CVD as an alternative for microcrystalline silicon in tandem and triple junction solar cells, Mater. Res. Soc. Symp. Proc. 1666 (2014) a01–a04.
[6] J. Yang, L. Newton, B. Fieselmann, Raman spectroscopy of a-SiGe:H alloys, Mater. Res. Soc. Symp. Proc. 149 (1989) 497–502.
[7] S.K. O'Leary, S.R. Johnson, P.K. Lim, The relationship between the distribution of electronic states and the optical absorption spectrum of an amorphous semiconductor: an empirical analysis, J. Appl. Phys. 82 (1997) 3334–3340.
[8] J. Tauc, Amorphous and Liquid Semiconductors, Plenum Press, London, 1974.
[9] K.F. Feenstra, Hot-wire Chemical Vapour Deposition of Amorphous Silicon and the Application in Solar Cells, Utrecht University, 1998. (Ph.D. thesis).
[10] D. Ritter, E. Zeldov, K. Weiser, Steady state photocarrier grating technique for diffusion length measurement in semiconductors, Appl. Phys. Lett. 49 (1986) 791–793.
[11] M.K. van Veen, R.E.I. Schropp, Beneficial effect of a low deposition temperature of hot-wire deposited intrinsic amorphous silicon for solar cells, J. Appl. Phys. 93 (2003) 121–125.
[12] Y.P. Chou, S.C. Lee, Structural, optical, and electrical properties of hydrogenated amorphous silicon germanium alloys, J. Appl. Phys. 83 (1998) 4111–4123.
[13] Y. Xu, A.H. Mahan, L.M. Gedvilas, R.C. Reedy, H.M. Branz, Deposition of photosensitive hydrogenated amorphous silicon–germanium films with a tantalum hot wire, Thin Solid Films 501 (2006) 198–201.
[14] W. Paul, D.K. Paul, B. von Roedern, J. Blake, S. Oguz, Preferential attachment of H in amorphous hydrogenated binary semiconductors and consequent inferior reduction of pseudogap state density, Phys. Rev. Lett. 46 (1981) 1016–1019.
[15] A. Terakawa, Hydrogenated Amorphous Silicon Germanium Alloys for High Efficiency and Stable Solar Cells, Kyoto University, 1999. (Ph.D. thesis).
[16] J. Folsch, F. Finger, T. Kulessa, F. Siebke, W. Beyer, H. Wagner, Improved ambipolar diffusion length in a-$Si_{1-x}Ge_x$:H alloys for multi-junction solar cells, MRS Symp. Proc. 377 (1995) 517–522.
[17] S. Hänni, G. Bugnon, G. Parascandolo, M. Boccard, J. Escarré, M. Despeisse, F. Meillaud, C. Ballif, High-efficiency microcrystalline silicon single-junction solar cells, Prog. Photovolt. Res. Appl. 21 (2013) 821–826.
[18] W. Reetz, T. Kirchartz, A. Lambertz, J. Hupkes, A. Gerber, Current–voltage and spectral response based characterization of thin film silicon solar cells — investigation of primary error sources, Proc. of the 24th Eu PVSEC Conference 2009, pp. 2784–2788.